Archives of Acoustics Vol. 48, No. 3, pp. 381–388 (2023), doi: 10.24425/aoa.2023.145244

Research Paper

Relationship Between the Sound Transmission Through the Finite Double-Panel Structure with a Cylindrical Shell Array and the Vibro-Acoustic Characteristics of its Constituents

Song-Hun KIM, Myong-Jin KIM*

Institute of Acoustics, Department of Physics, Kim Il Sung University
Pyongyang, Democratic People's Republic of Korea

*Corresponding Author e-mail: mj.kim0903@ryongnamsan.edu.kp

(*received February 23, 2022; accepted February 7, 2023*)

Sound insulation of the finite double-panel structure (DPS) inserted with a cylindrical shell array is investigated by varying the sound incidence direction to improve its applicability. The effects of the vibro-acoustic characteristics of its constituents on the sound transmission loss (STL) are estimated in one-third octave bands from 20 Hz to 5 kHz for different incidence conditions. It shows that the first acoustic mode in the direction parallel to two panels (longitudinal modes) produces both the sudden variation of sound insulation with frequency and a large dependency on the incidence angle. Mineral wools are placed on two boundaries perpendicular to the panels, and the sound insulation is explored for different thicknesses of the porous materials. An absorbent layer with a certain thickness (more than 30 mm in our work) sufficiently eliminates the longitudinal mode, resulting in the improvement in the sound insulation by more than 15 dB and the decrease of its large variation with incidence direction. STLs with varying shell thicknesses are also assessed. It shows that the natural vibrations of the thin shells can give an enhancement in sound insulation by more than 10 dB in the frequency range of 1600–3700 Hz, corresponding to constructive interference.

Keywords: sound transmission loss; double-panel structure; eigenmode vibration; sonic crystal.

1. Introduction

It was first found experimentally in 1995 that the periodic arrangement of scatterers gives a high acoustic attenuation in the frequency range centered around Bragg's frequency (Martínez-Sala *et al.*, 1995). Since then, several studies have been performed to control the noise using a cylindrical solid array.

The acoustical band structure of the regularly arranged solid cylinders in the free field was predicted by the plane wave expansion (PWE) method (Chen, Ye, 2001; Romero-García *et al.*, 2011) and multiple scattering theory (MST) (Krynkin *et al.*, 2011) and validated experimentally. Martínez-Sala *et al.* (2006) conducted a free field measurement on the tree arrangement similar to the periodic lattice and showed that it behaves like a sonic crystal (SC), its acoustic attenuation is higher than those for the ordinary forest and grass in the frequency range below 500 Hz, and it has the practical possibility to be used as a green noise barrier. Sound attenuations through the solid cylinder arranged in periodic arrays were investigated using the coupling of Bragg-type reflection and the sound absorption caused by placing the absorbents, such as porous material, on the scatterers or filling the gaps between them (Umnova *et al.*, 2006; Sánchez-Dehesa *et al.*, 2011).

Inserting an SC between two panels can improve the sound insulation of the structure in the audible frequency range. Tang (2018) reported that installing cylinder columns into a plenum window gave rise to a broadband improvement in noise reduction. The author also investigated the effect of parameters such as the number and location of columns, lattice arrangement, and so on. Gulia and Gupta (2018) estimated the individual and coupling effects of SC and porous material inserted into double-panel structure (DPS) and found that the coupling of two elements gave the highest sound insulation. Kim (2019a) extended the work of Gulia and Gupta (2018) to the triple-panel

structure and showed that it exhibited higher sound insulation than DPS with the same total thickness and mass over the entire frequency range, even giving a potential to reduce the overall weight.

Using the local resonance effect is one way to reduce sound transmission in the low-frequency range or in the frequency range of interest without increasing the thickness and weight. Chalmers *et al.* (2009) suggested two types of SCs comprised of C-shaped Helmholtz resonators: the first is simply mixing two columns with different resonance frequencies, and the second is the arrangement of concentric resonators. Elford *et al.* (2011) presented a six concentric Matryoshka configuration of slit cylinders. Simulation results demonstrated the overlapping of the individual resonance peaks in the low-frequency range and the broadening of the resonant band gap. Local resonant SCs comprised of thin elastic shells were also presented, in which the breathing mode resonance of the shell was used. Krynkin *et al.* (2010) showed that the periodic arrangement of the thin elastic shells made of soft rubber exhibits a wide band gap due to the axisymmetric resonance in the shell. Fuster-Garcia *et al.* (2007) demonstrated experimentally the resonant behavior of an array formed with pressurized gas-filled balloons and the possibility of achieving a full band gap in a desired frequency range. Chong (2012) presented a study on the sound insulation of a noise barrier consisting of a concentric arrangement of an outer 4-slit rigid cylinder and an inner elastic cylindrical shell.

Local resonant SCs were applied to the multiple-panel structure to enhance the sound insulation. Kim (2019b) proposed an array of C-shaped scatterers with different Helmholtz resonance frequencies and showed that the DPS with the array gave a relatively wide band gap in the low-frequency range. Gulia and Gupta (2019) showed that coupling the effects of the local resonant SC and porous material in the triple panel gave better sound transmission loss (STL) in the low-frequency range as well as in the high-frequency range. Kim *et al.* (2021) formed the resonant band gap in the low-frequency range by using the local resonant SC comprised of slot-type resonators, in which the slots were elongated into the cavity and had different depths.

Normal incidence condition is usually applied to the inlet of SC for numerical and analytical research, including the calculation of the acoustic band structure, the prediction of STL and the optimization. In addition, its dimension is considered infinite and the periodicity condition is used to reduce the computing cost. For the cylindrical scatterers, sound hard condition is applied to their surfaces, leading to no accounting for the effect of shell vibration on the sound propagation.

In this work, variation of the sound insulation through a DPS with a periodic arrangement of cylindrical shells is systematically investigated with varying the incidence angle of sound waves. Particularly, the dependency of sound insulation on the incidence direction is analyzed in relation to the acoustic mode of the finite air cavity. By weakening the longitudinal acoustic mode using the sound-absorbing material of a certain thickness, the large variation in STL with frequency is eliminated and the sound insulation is improved. Varying the shell thickness, the sound insulations are estimated in the frequency range where the scattered waves interfere constructively. Structural and acoustical characteristics of the entire structure and its constituents are analyzed using the VA One v.2015 software for analysis and design of vibro-acoustic systems.

2. Numerical modeling

A schematic diagram of DPSs with a periodic arrangement of the cylindrical shells is shown in Fig. 1. Figure 1a presents the DPS without any sound absorbent and Fig. 1b shows the one with the absorbent on two boundaries in the longitudinal direction (upper and lower in the figure).

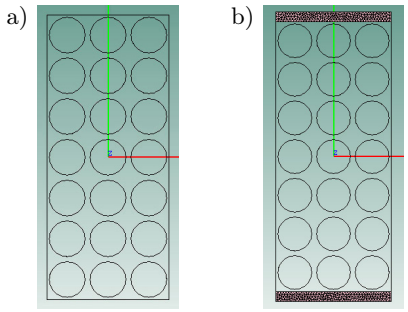

Fig. 1. DPSs with a cylindrical shell array: a) without absorbent; b) with absorbent.

Cylindrical shells are arranged on a 7×3 square lattice, and they are inserted between two parallel panels, as shown in Fig. 1. Distance between the two centers of the neighboring shells (lattice constant) is 40 mm and the outer diameter of the shell is 35 mm. The left side of the DPS is the aluminum panel with a thickness of 4 mm, and the right side is the plywood panel with a thickness of 5 mm. Cylindrical shells are considered to be made of aluminum. The sound speed in air is $c_0 = 343$ m/s, the density of air $\rho_0 = 1.25$ kg/m^3, and the material properties of aluminum and plywood are presented in Table 1.

Table 1. Material properties of aluminum and plywood.

	Density [kg/m^3]	Young's modulus [GPa]	Poisson's ratio
Aluminum	2700	71	0.33
Plywood	700	6	0.25

Table 2. Non-acoustic properties of mineral wool.

Flow resistivity [N·s/m^4]	Porosity	Tortuosity	Viscous characteristic length [m]	Thermal characteristic length [m]
6×10^4	0.95	3.2	5×10^{-5}	1.06×10^{-4}

The DPS is mounted in an infinite baffle and sound waves are incident on the left side (i.e., aluminum panel with a thickness of 4 mm). The acoustic velocity is zero in the infinite baffle. The infinite air regions on both sides of the DPS are modeled using the boundary element method (BEM). Sound hard condition is applied to the upper and lower boundaries of the air region between the two panels. Sound waves are completely reflected by such boundaries, and the particle velocity perpendicular to the boundaries is zero as expressed by Eq. (1) (Gulia, Gupta, 2018):

$$\left(-\frac{\nabla p}{\rho}\right)\cdot\mathbf{n}=0, \tag{1}$$

where p and $\mathbf{n}$ denote the sound pressure and normal vector, respectively.

For harmonic excitation, the vibration displacement of the panel can be expanded on the basis of eigenfunctions ψ_{mn}, which satisfy the following equation (Bruneau, 2006):

$$\left(\frac{\partial^4}{\partial x^4}+2\frac{\partial^4}{\partial x^2\partial y^2}+\frac{\partial^4}{\partial y^4}-k_{mn}^2\right)\psi_{mn}=0, \tag{2}$$

where $k_{mn}^2=\omega_{mn}^2M_s/B$, $M_s=\rho_p h$, $B=Eh^3/12(1-\nu^2)$, ω_{mn}, M_s, and B represent the natural angular frequency, the mass per unit area and the bending stiffness, respectively, and ρ_p, ν, h, and E are the density, Poisson's ratio, the thickness, and Young's modulus of the panel, respectively.

For the simply supported rectangular panel, the displacement and bending moment are zero at the boundaries and the natural angular frequencies are as follows:

$$\omega_{mn}=\sqrt{\frac{B}{M_s}}\left[\left(\frac{m\pi}{w}\right)^2+\left(\frac{n\pi}{l}\right)^2\right], \tag{3}$$

where w and l are the width and length of the panel, respectively.

Because the identical shells are arranged periodically, a high and wide band gap is formed around the Bragg frequency (Eq. (4)) due to the destructive interference of the scattered waves:

$$f_B=\frac{c}{2a}, \tag{4}$$

where a is the lattice constant and c is the sound speed in air. On the contrary, the sound insulation around the frequency corresponding to half the Bragg frequency tends to get worse compared to that without the scatterer array due to constructive interference (Gulia, Gupta, 2018; Kim, 2019a; Kim *et al.*, 2021).

A porous material is one of the most widely used absorbents for noise control. In this work, porous materials with different thicknesses were placed on the upper and lower boundaries of the DPS. Mineral wool is taken as a porous material and an equivalent fluid model-limp porous model (Allard, Atalla, 2009) is used to describe the sound propagation in the mineral wool. The limp model of the porous material is valid when the thin light foam is decoupled with an air gap from a vibrating system. This model requires the evaluation of the acoustic and non-acoustic (or microscopic) properties. The acoustic property is sound absorbing efficiency, while there are five non-acoustic properties, including static airflow resistivity, porosity, tortuosity, viscous characteristic length, and thermal characteristic length.

Similar to other porous materials, the absorption coefficient of mineral wool also increases with increasing thickness. The density of the mineral wool is 50 kg/m^3, and its non-acoustic properties are presented in Table 2.

Harmonic analyses are performed to estimate STLs in the 1/3 octave bands covering the range from 20 Hz to 5 kHz. For the sake of reducing the computing cost, two-dimensional analyses are conducted, considering the length of shells to be large enough compared to the outer diameter and thickness. Acoustical and structural constituents are modeled using the finite element method (FEM), while the fluid medium (air) is modeled using the BEM. STL is taken as the difference in sound power levels at the 4 mm-thick aluminum panel and the 5 mm-thick plywood panel.

3. Results and discussion

Figure 2 shows the STLs in 1/3 octave bands for two cases of the incidence angles, 10 and 90°, between the panel surface and the sound incidence direction. For the incidence angles from 10 to 90°, STLs lie mainly between the two curves. In the figure, STL for diffused field incidence is also plotted.

The frequency range below 100 Hz can be considered as the stiffness-controlled portion in Fig. 2. The range from 100 to 200 Hz corresponds to the first resonances of the two panels. The first resonance frequencies of two panels are 84.6 and 118.7 Hz, respectively, leading to the high sound transmission in the frequency range.

STLs increase rapidly for the frequency range over 4 kHz and then become higher than 110 dB at 5 kHz.

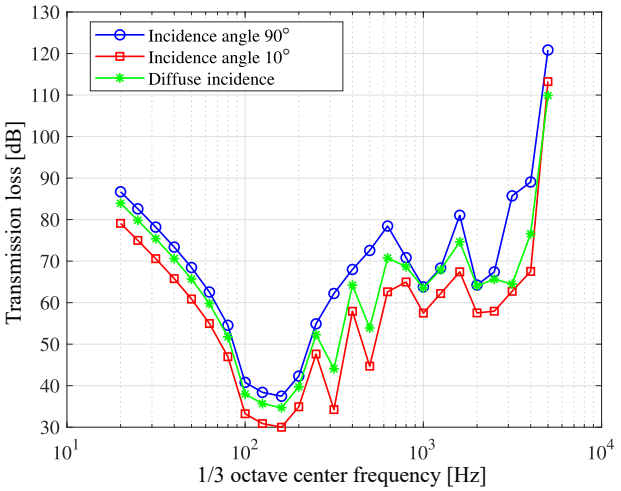

Fig. 2. STLs in 1/3 octave bands.

This corresponds to the Bragg band gap due to the periodic arrangement of cylindrical shells between two panels with a lattice constant of 40 mm. According to Eq. (4), the Bragg band gap is centered at 4287.5 Hz.

The sound insulation of the DPS gets higher when the incidence angle increases, and the STL for the diffused incidence falls approximately in between the values observed for two extreme cases (10 and 90°).

The variation width in STL with the incident angle is shown in Fig. 3. The variation in STL is uniform around 7.5 dB in the frequency range from 20 to 250 Hz, but large above that. Especially it is particularly large in the frequency ranges of 250 to 630 Hz and 2 to 4 kHz.

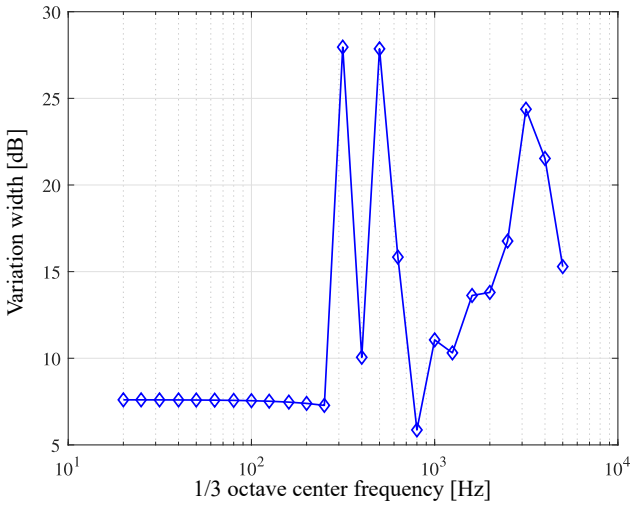

Fig. 3. Variation width in STL as a function of 1/3 octave band.

Since both the acoustic and structural elements of the DPS have finite dimensions, there are acoustic and structural eigenmodes in different directions.

Figure 4 shows the number of acoustic modes generated in the air region surrounded by cylindrical shells,

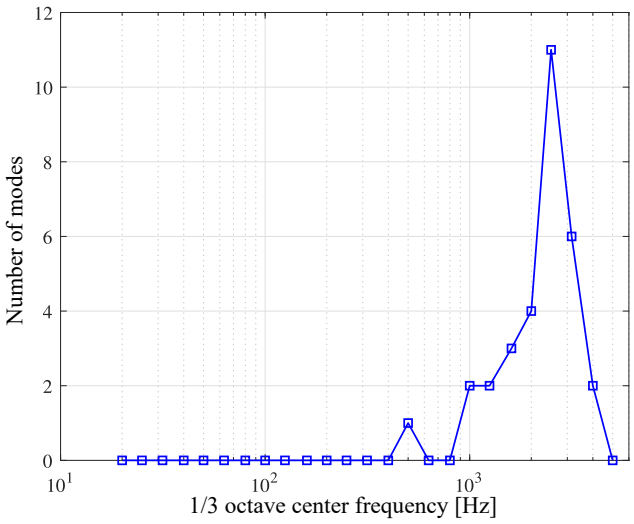

Fig. 4. Numbers of acoustic modes in 1/3 octave bands.

two parallel panels, and upper and lower boundaries. There is no acoustic mode in the frequency range below 400 Hz, and one mode exists in the 1/3 octave band with a center frequency of 500 Hz. For the frequencies above 1 kHz, the number of acoustic modes increases gradually, reaching a maximum of 11 in the band centered at 2500 Hz. Then, it decreases rapidly and becomes zero again at 5 kHz.

There are three types of acoustic eigenmodes: transverse, longitudinal, and coupled ones. Figure 5 shows four natural acoustic modes with frequencies of 469.9, 929.9, 1079.2, and 1182 Hz, respectively.

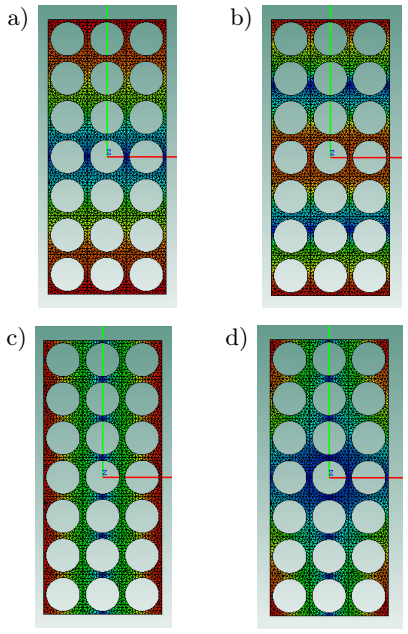

Fig. 5. Acoustic modes: a) 469.9 Hz; b) 929.9 Hz; c) 1079.2 Hz; d) 1182 Hz.

In the figure, 469.9 Hz corresponds to the first longitudinal mode, 929.9 Hz to the second longitudinal mode,

1079.2 Hz to the first transverse mode, and 1182 Hz to the coupled mode. Such acoustic modes provide different contributions to sound transmission through the DPS according to the incidence angle.

For a given incidence angle of 10°, four acoustic modes are suppressed one after another and the results are presented in Fig. 6. As presented in the figure, suppressing the first longitudinal mode eliminates the large fluctuations in sound insulation in the range from 250 to 630 Hz and STL increases monotonically. Considering the fact that the first longitudinal mode is in the range from 250 to 630 Hz, it can be seen that the large reduction and strong fluctuation in sound insulation are caused by the first eigenmode. The more the incident sound wave is inclined, the stronger the excitation of the first longitudinal mode becomes. Then, the scattering of sound waves by the cylindrical shells becomes stronger, resulting in an increase in sound energy radiated from the output surface of the DPS.

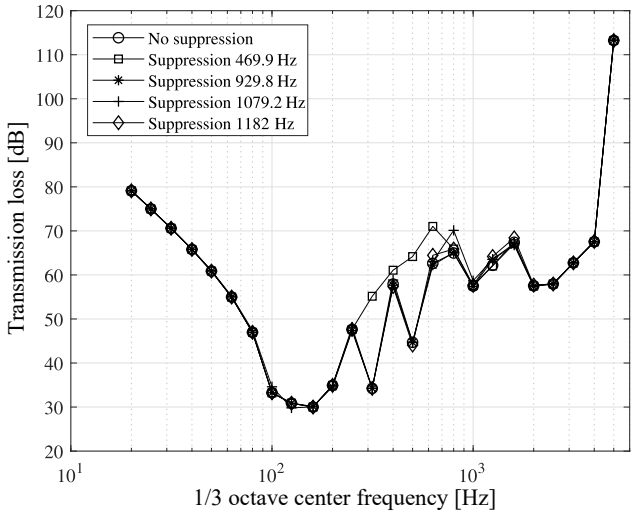

Fig. 6. STLs in 1/3 octave bands for an incidence angle of 10°.

For the other cases of 929.9, 1079.2, and 1182 Hz, the sound insulation is improved by about 1 dB in the frequency range from 630 to 1250 Hz and there is no change in STL in the remaining range. As shown in Fig. 4, there are a relatively large number of natural acoustic modes in the frequency range from 2 to 4 kHz, so it can be understood that the addition of effects of the individual modes results in a large variation in STL in the frequency range. From these behaviors, it can be concluded that, for a sound wave obliquely incident on the boundary of DPS, the first longitudinal acoustic mode produces the largest influence on its sound insulation. On the other hand, the influences of the remaining modes are very small compared to that of the first longitudinal mode.

In order to eliminate the remarkable variation and reduction in STL in the frequency range from 250 to 630 Hz, it is necessary to reduce the intensity of the first longitudinal mode using the sound-absorbing materials. To confirm this, mineral wools with non-acoustic properties, as shown in Table 2, are placed on the upper and lower boundaries, as in Fig. 1b, and then STLs are evaluated for three different thicknesses of mineral wool. The absorption coefficients of the mineral wool are shown in Fig. 7.

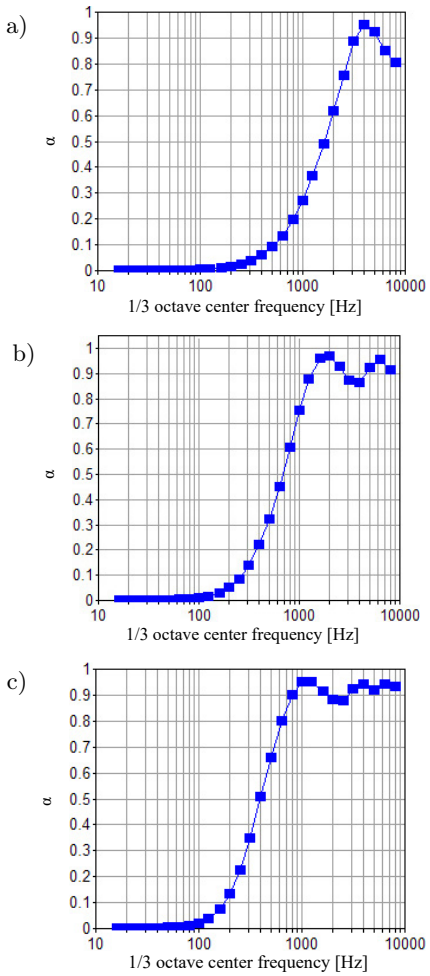

Fig. 7. Absorption coefficient of mineral wool thickness: a) 10 mm; b) 20 mm; c) 30 mm.

Similar to other porous materials, the sound absorption coefficient of mineral wool is very small at low frequencies and relatively great at high frequencies. As shown in Fig. 7, the absorption coefficient is smaller than 10% at frequencies below 500 Hz for a thickness of 10 mm. With increasing thickness, the absorption peak shifts towards the lower frequencies, and for a thickness of 30 mm, the absorption coefficient is greater than 10% at 200 Hz and increases rapidly beyond that frequency.

Figure 8 shows STLs with various thicknesses of mineral wool for an incidence angle of 10°.

Increasing the absorbent thickness not only reduces the unexpected fluctuation in STL with frequency, but also significantly enhances the sound insulation in the

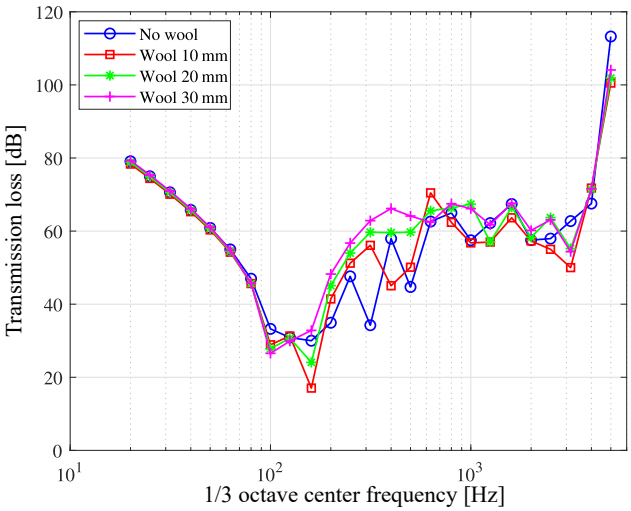

Fig. 8. STL with various thicknesses of absorbing material for an incidence angle of 10°.

frequency range of interest. Especially, the sound insulation for a thickness of 30 mm is higher than that without absorbing materials approximately at all the bands and the variation width in SPF with the incidence angle decreases to less than 10 dB.

Figure 9 shows STLs with varying thicknesses of the mineral wool for diffused field incidence. Similar to the above case of the incidence angle of 10°, placing the absorbent of thickness 30 mm improves the overall sound insulation and completely eliminates the abrupt change in STL in the frequency range from 250 to 630 Hz. From these results, it can be concluded that the variation in STL through DPS with the incidence direction of a sound wave is primarily caused by the longitudinal acoustic modes in the direction parallel to the panel surface of DPS. And a certain thickness of absorbent is required not only to decrease the strong dependency of STL on the incidence angle but also to improve the overall sound insulation.

The cylindrical shell can be made either of polyvinyl chloride (PVC) or sheet metal. In the case of cylindrical shells with finite thickness, they will oscillate by acoustic loading and consequently would have some influences on the sound propagation through DPS.

Figure 10 shows the overall sound power transmitted through the DPS in the frequency range from 20 Hz to 5 kHz when the thickness of the cylindrical shell, made of aluminum, varies from 0.2 to 2 mm. The sound wave is diffusely incident on the DPS and the amplitude of the sound pressure in all directions is 1 Pa.

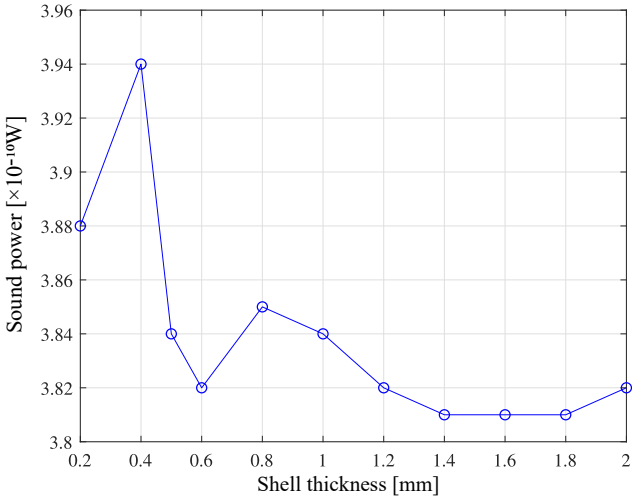

Fig. 10. Overall transmitted sound power as a function of shell thickness.

In Fig. 11, the overall transmitted sound power is a maximum for the shell thickness of 0.4 mm and approximately decreases with increasing the shell thickness. It has little variation above 1.4 mm, which means that vibration displacement can be regarded as almost zero for acoustic loading. Although the overall trans-

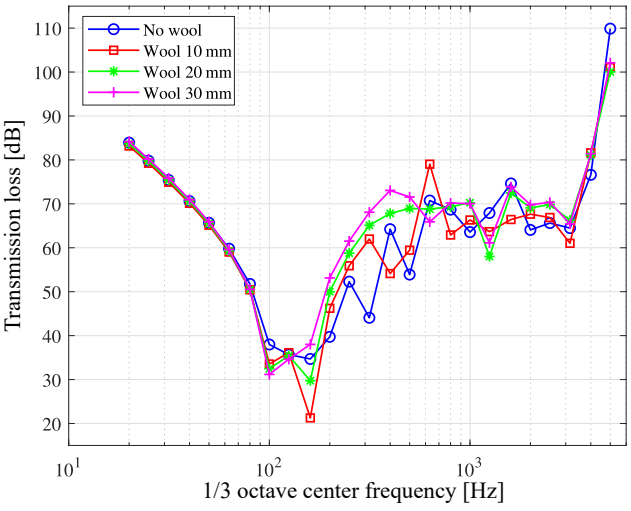

Fig. 9. STL with various thicknesses of absorbing material for diffused incidence.

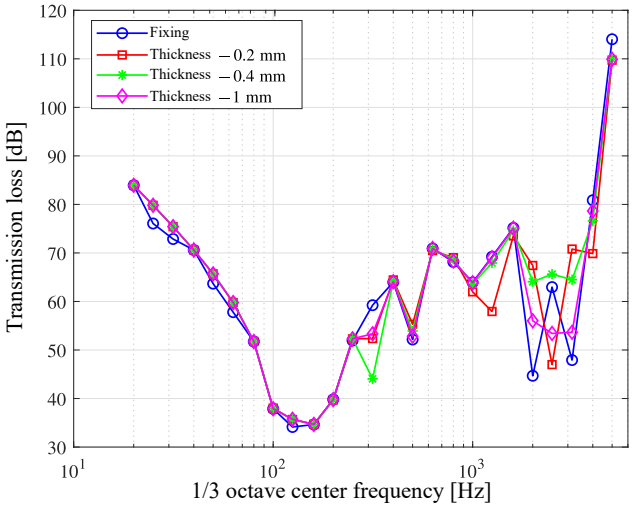

Fig. 11. STLs with various shell thicknesses.

mitted sound power varies with the shell thickness, its variation width is negligibly small on a logarithmic scale (about 0.15 dB). But, the individual ones in 1/3 bands might be significantly different from each other when the shell thickness varies.

Figure 11 shows STLs for three cases with shell thicknesses of 0.2, 0.4, and 1 mm. STL for the DPS with perfectly fixed shells is also shown in the figure. Differences in the STLs between the four cases are small except in the frequency ranges below 1600 and above 3700 Hz, where the sound insulation varies greatly with the shell thickness and is lower than those in the two adjacent frequency bands, even lower than that without the shell array. This result was already reported in previous research (Gulia, Gupta, 2018; 2019; Kim, 2019a; Kim *et al.*, 2021).

The reason for this is that the range is around the frequency at which the lattice constant is equal to 1/4 of the wavelength and thus the acoustic waves scattered by periodic cylindrical shells constructively interfere with each other.

In the figure, the sound insulation in the frequency range from 1600 to 3700 Hz is the highest for the shell thickness of 0.4 mm, and it is up to 10 dB higher than the other cases in the frequency range.

The natural frequencies in the entire frequency range from 20 Hz to 5 kHz are shown in Table 3 for different shell thicknesses. In all the cases, the cylindrical shells exhibit one or two natural frequencies in the frequency range from 1600 to 3700 Hz.

Table 3. Natural frequencies of shells with various shell thicknesses.

Shell thickness [mm]	Natural frequency [Hz]
0.2	431, 1220, 2344, 3796
0.4	852, 2413, 4634
0.6	1269, 3593
0.8	1685, 4769
1	2100

As shown in Fig. 11, the even-order mode (2413 Hz for shell thickness of 0.4 mm) disturbs the constructive interferences of the acoustic waves scattered by the shells, resulting in an improvement of the sound insulation in the frequency range from 1600 to 3700 Hz. On the contrary, the odd-order modes (2344 Hz for shell thickness of 0.2 mm and 2100 Hz for shell thickness of 1 mm) exhibit no improvements in the sound insulation; instead, they negatively contribute to the sound insulation, as shown in Fig. 11.

4. Conclusions

The effects of the structural and acoustic modes on sound transmission through a finite-size DPS were evaluated and analyzed. For the inclined incidence, STLs strongly vary around the frequency (489.9 Hz in this work) corresponding to the first longitudinal mode in the direction parallel to the panel surface of DPS, resulting in poor sound insulation. The variation in the sound insulation with incidence angle is also the largest around that frequency. With varying the incidence angle of sound waves from 10 to 90°, the sound insulation changes within 7 to 8 dB in most 1/3 octave bands, but it has a variation width of even more than 25 dB in some bands around that frequency. The first longitudinal acoustic mode gives the largest effect on the sound insulation and those of the other acoustic modes are very small. Placing the mineral wool of a certain thickness (30 mm in this work) on two longitudinal boundaries can significantly suppress the intensity of the first longitudinal acoustic mode. This exhibits a reduction of the variation in STL with an incident angle to less than 10 dB and an increase of the sound insulation by more than 15 dB in the frequency range around the mode (250 to 630 Hz in this work). Cylindrical shells can have their natural vibration modes in the frequency range where the sound waves scattered by the shells interfere constructively. Even-order modes of them behave to disturb the constructive interferences of the scattered waves, which can greatly enhance the sound insulation through the DPS in the frequency range (1600 to 3700 Hz in this work). On the other hand, the odd-order modes have negative effects on sound insulation.

Acknowledgments

The authors would like to express their gratitude to professors and researchers in the Department of Physics at Kim Il Sung University for their great opinions, discussions, and constructive assistance in improving the scientific value and quality of this work.

References

1. Allard J.F., Atalla N. (2009), *Propagation of Sound in Porous Media: Modeling Sound Absorbing Materials*, 2nd ed., John Wiley & Sons, doi: 10.1002/9780470747339.

2. Bruneau M. (2006), *Fundamentals of Acoustics*, ISTE Ltd Press, London.

3. Chalmers L., Elford D.P., Kusmartsev F.V., Swallowe G.M. (2009), Acoustic band gap formation in two-dimensional locally resonant sonic crystals comprised of Helmholtz resonators, *International Journal of Modern Physics B*, **24**(20n21): 4231–4243, doi: 10.1142/S0217979209063390.

4. Chen Y.-Y., Ye Z. (2001), Acoustic attenuation by two-dimensional arrays of rigid cylinders, *Physical Re-*

view Letters, **87**(18): 184301, doi: 10.1103/PhysRevLett.87.184301.

5. Chong Y.B. (2012), *Sonic crystal noise barriers*, Ph.D. Thesis, The Open University, Milton Keynes, UK, doi: 10.21954/ou.ro.0000add6.

6. Elford D.P., Chalmers L., Kusmartsev F.V., Swallowe G.M. (2011), Matryoshka locally resonant sonic crystal, *The Journal of the Acoustical Society of America*, **130**(5): 2746–2755, doi: 10.1121/1.3643818.

7. Fuster-Garcia E., Romero-García V., Sánchez-Pérez J.V., García-Raffi L.M. (2007), Targeted band gap creation using mixed sonic crystal arrays including resonators and rigid scatterers, *Applied Physics Letter*, **90**(24): 244104, doi: 10.1063/1.2748853.

8. Gulia P., Gupta A. (2018), Enhancing the sound transmission loss through acoustic double panel using sonic crystal and porous material, *The Journal of the Acoustical Society of America*, **144**(3): 1435–1442, doi: 10.1121/1.5054296.

9. Gulia P., Gupta A. (2019), Sound attenuation in triple panel using locally resonant sonic crystal and porous material, *Applied Acoustics*, **156**: 113–119, doi: 10.1016/j.apacoust.2019.07.012.

10. Kim M.-J. (2019a), Improving sound transmission through triple-panel structure using porous material and sonic crystal, *Archives of Acoustics*, **44**(3): 533–541, doi: 10.24425/aoa.2019.129268.

11. Kim M.-J. (2019b), Numerical study for increasement of low frequency sound insulation of double-panel structure using sonic crystals with distributed Helmholtz resonators, *International Journal of Modern Physics B*, **33**(14): 1950138, doi: 10.1142/S0217979219501388.

12. Kim M.-J., Rim C.-G., Won K.-S. (2021), Broadening low-frequency band gap of double-panel structure using locally resonant sonic crystal comprised of slot-type Helmholtz resonators, *Archives of Acoustics*, **46**(2): 335–340, doi: 10.24425/aoa.2021.136587.

13. Krynkin A., Umnova O., Yung Boon Chong A., Taherzadeh S., Attenborough K. (2010), Predictions and measurements of sound transmission through a periodic array of elastic shells in air, *The Journal of the Acoustical Society of America*, **128**(6): 3496–3506, doi: 10.1121/1.3506342.

14. Krynkin A., Umnova O., Sánchez-Pérez J.V., Yung Boon Chong A., Taherzadeh S., Attenborough K. (2011), Acoustic insertion loss due to two dimensional periodic arrays of circular cylinders parallel to a nearby surface, *The Journal of the Acoustical Society of America*, **130**(6): 3736–3745, doi: 10.1121/1.3655880.

15. Martínez-Sala R., Rubio C., García-Raffi L.M., Sánchez-Pérez J.V., Sánchez-Pérez E.A., Llinares J. (2006), Control of noise by trees arranged like sonic crystals, *Journal of Sound and Vibration,* **291**(1–2): 100–106, doi: 10.1016/j.jsv.2005.05.030.

16. Martínez-Sala R., Sancho J., Sánchez J.V., Gómez V., Llinares J., Meseguer F. (1995), Sound attenuation by sculpture, *Nature*, **378**: 241, doi: 10.1038/378241a0.

17. Romero-García V., Garcia-Raffi L.M., Sánchez-Pérez J.V. (2011), Evanescent waves and deaf bands in sonic crystals, *AIP Advances*, **1**(4): 041601, doi: 10.1063/1.3675801.

18. Sánchez-Dehesa J., Garcia-Chocano V.M., Torrent D., Cervera F., Cabrera S., Simon F. (2011), Noise control by sonic crystal barriers made of recycled material, *The Journal of the Acoustical Society of America*, **129**(3): 1173–1183, doi: 10.1121/1.3531815.

19. Tang S.K. (2018), Reduction of sound transmission across plenum windows by incorporating an array of rigid cylinders, *Journal of Sound and Vibration*, **415**: 25–40, doi: 10.1016/j.jsv.2017.11.027.

20. Umnova O., Attenborough K., Linton C.M. (2006), Effects of porous covering on sound attenuation by periodic arrays of cylinders, *The Journal of the Acoustical Society of America*, **119**(1): 278–284, doi: 10.1121/1.2133715.